Molecular Crystals and Liquid Crystals
Publication details, including instructions for authors and subscription information:
http://www.tandfonline.com/loi/gmcl20

Relating Display Performance and Grating Structure of a Zenithal Bistable Display

J. C. Jones [a] & R. M. Amos [a]
[a] ZBD Displays Ltd., Malvern Hills Science Park, Malvern, Worcestershire, UK

Version of record first published: 14 Jun 2011

To cite this article: J. C. Jones & R. M. Amos (2011): Relating Display Performance and Grating Structure of a Zenithal Bistable Display, Molecular Crystals and Liquid Crystals, 543:1, 57/[823]-68/[834]

To link to this article: http://dx.doi.org/10.1080/15421406.2011.568330

Mol. Cryst. Liq. Cryst., Vol. 543: pp. 57/[823]–68/[834], 2011

ISSN: 1542-1406 print/1563-5287 online
DOI: 10.1080/15421406.2011.568330

Taylor & Francis
Taylor & Francis Group

Relating Display Performance and Grating Structure of a Zenithal Bistable Display

J. C. JONES AND R. M. AMOS

ZBD Displays Ltd., Malvern Hills Science Park, Malvern, Worcestershire, UK

Zenithal Bistable Devices use a deep homeotropic grating as one of the alignment layers to induce two stable surface pre-tilts. Attributes of the display such as operating voltage, temperature range, and optical properties depend on the shape and anchoring properties of the grating. Understanding these relationships enables devices with improved performance to be designed and fabricated.

Keywords Bistability; electro-optic effects; flexoelectricity; grating alignment; liquid crystal displays; Zenithal Bistable Devices; Zenithal Bistable Display

1. Introduction

An important factor for all commercial liquid crystal devices is the alignment layers, and optimising the performance of such devices involves ensuring the correct alignment layers are used. No where is this more evident than for the Zenithal Bistable Device [1,2] from ZBD: such devices have a similar design to conventional Twisted Nematic LCDs, except that one of the alignment surfaces is formed from a zenithally bistable grating structure, rather than the standard rubbed polymer. The device gives low voltage operation for standard 7 μm spacing; construction is readily made on standard production lines and uses conventional nematic liquid crystal mixtures, polarisers and electronic drivers. This type of display is ideal for Electronic Shelf Edge labels in the retail sector because they combine high legibility and image content with zero power consumption when not being updated. When combined with ZBD's RF protocol, labels can operate continuously from two button batteries for up to 7 years when updated several times each day, despite two way communication for each label with a single transceiver in the store. These attributes are leading to rapidly increasing deployment of ZBD's retail label solution across Europe.

The display design used in the commercial labels is shown in the Figure 1. The grating is designed to impose either a high tilt or low tilt state upon the adjacent liquid crystal. The simplest example of such a zenithally bistable surface uses a grating with a locally homeotropic boundary condition to force the elastic deformation of the liquid crystal director close to that surface. Bistability results if the pitch and

Address correspondence to J. C. Jones, ZBD Displays Ltd., Malvern Hills Science Park, Malvern, Worcestershire, UK. Tel.: +44-1684 585313; Fax: +44-1684 585390; E-mail: jcjones@zbd.co.uk

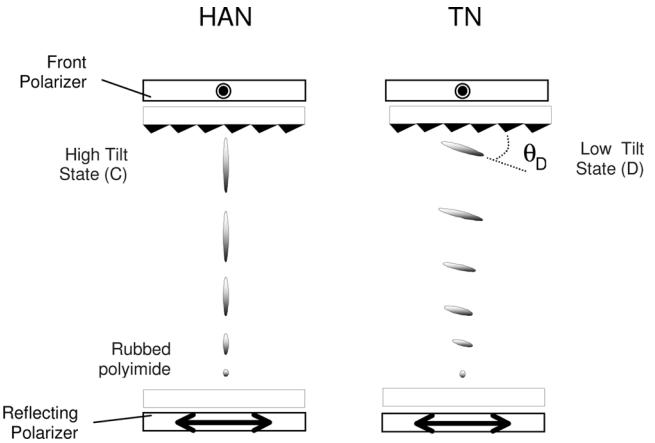

Figure 1. Operating principal of a ZBD^{TM} Display.

depth dimensions of the grating are similar. The low tilt state is termed the D state due to the +/− ½ disclination loops of the director field at the top and the bottom of the grating grooves, whereas the high tilt state is termed C, because the director field is continuous and devoid of defects. Latching between the states is done using polar fields that couple to the flexo-electric surface polarisation induced by the elastic deformations close to the grating surface. Bistability and latching both result from the properties of the grating surface. Hence, the bistable grating can be used with a variety of different LCD geometries, including the Pi-cell, HAN-VAN and TN to VAN geometries. Current commercial devices have the grating direction parallel to the rubbing direction on the opposing surface to give latching between the 90° TN for the low tilt D state and the hybrid aligned or HAN state for the high tilt C state. This arrangement combines the excellent reflectivity of the TN state, with the contrast and viewing angle allowed by the TN – HAN combination. The excellent appearance is achieved without the need for compensation layers, and the tolerance on the 7 μm cell gap is lenient (typically ±0.25 μm rather than the ±0.05 μm of STN). Latching occurs for pulse magnitudes of several volts, and durations around 100 microseconds. This means that the display is readily addressed using conventional STN drivers, and the image typically takes a few hundred milliseconds to update.

In the current work, the relationship between device properties and grating structure will be reviewed. In particular, the latching voltage between the C and D states, the temperature range over which bistability is maintained and the pre-tilt of the D state will each be related to the grating shape and surface anchoring energy.

2. Latching Model

Latching between the bistable states involves nucleation and annihilation of +/−½ disclinations on a profiled surface with finite anchoring. The electric field couples to the nematic flexoelectric polarization induced close to the surface as the director is forced into elastically deformed states by the anchoring condition of the surface. The magnitude of the flexoelectric polarization is in turn related to the dielectric and visco-elastic properties of the liquid crystal due to the conventional re-orientation of

the director related to E^2. Such a complex two-dimensional system requires numerical modeling, and the method chosen is a 2D lattice Boltzmann solution to the Q-tensor of reference [3], using the Qian-Sheng approach to defect creation and annihilation. Theoretical comparison of the latching voltages for practical devices is done for the first time in [4].

Figure 2 shows a set of simplified snapshots of the 2D director field close to the grating with an applied bi-polar electric field. The polarity of the field favours the transition from the C state to D state. The first portion of the applied electric field distorts the director from low tilt in the bulk to near vertical due to coupling to the strongly positive $\Delta\varepsilon$. This increases the flexoelectric polarization close to the grating surface. As the polarity of the field is reversed, a defect pair is created at the point-of-inflexion on the grating surface; the flexo-electric polarization causes the $-1/2$ defect to move in the direction of the applied field towards the grating apex and the $+1/2$ defect to move in the opposite direction towards the grating trough. Once past a certain separation on the surface, the defect pair will continue to the top and bottom of the grooves through the influence of the surface curvature. That is, the $-1/2$ defect is favoured by the concave surface at the apex, and is repelled by the convex surface of the grating groove, and *vice-versa* for the $+1/2$ defect. Once at the point of no-return, the device can be said to be latched from the C into the D state: even if the electrical pulse is removed the D state will be retained. This may occur even if the defects have not fully reached their final stable positions because of the effect of the surface curvature. Also, the director in the bulk of the cell may also continue to relax into the new state dictated by that required by the surface after latching. In commercial devices, a pixel may be latched into a new state within 100 µs, though the optical change associated with this (say, from black to white) may take 100 ms.

Latching from D to C is the reverse of Figure 2, though in this instance the surface director begins in the vertical state and is less affected by the initial distortion. For this reason, the optical transition for this transition (say, from white to black) is much faster.

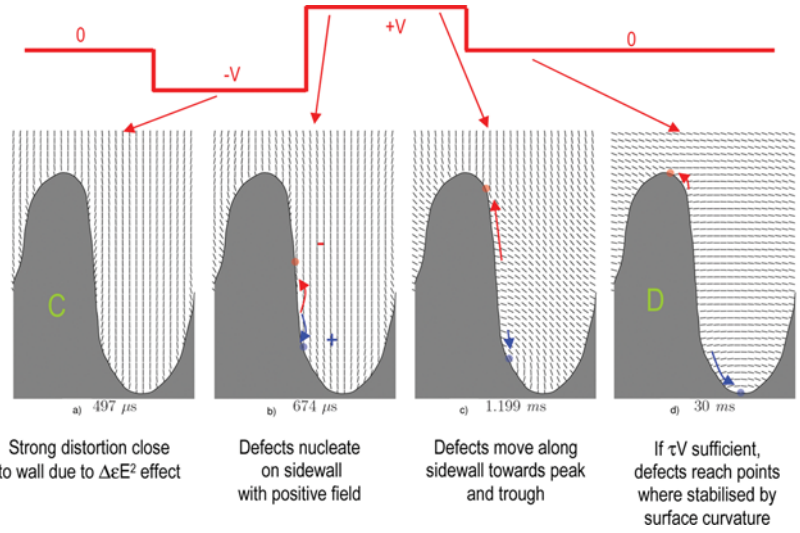

Figure 2. Snapshots from the numerical modelling of reference [4] for the C to D transition in response to an applied bipolar electric pulse. (Figure appears in color online.)

When designing devices, it is convenient to consider a simple one-dimensional model. In this instance, we may consider that there is a surface polarisation that couples to the applied electric field, inducing latching between high and low pre-tilt states once the elastic deformation exceeds a critical torque. Such a model has been investigated by Davidson and Mottram [5]. Simplifying that treatment still further to the case of high $\Delta\varepsilon$ and bipolar pulses (wherein latching starts from the vertical state for both transitions) leads to the following approximation [4]:

$$V_{CD} = \frac{\gamma_1 l_s \cdot d}{(e_{11} + e_{33})\tau_i} + \frac{2W_\theta}{(e_{11} + e_{33}) + \sqrt{\varepsilon_0 \Delta\varepsilon K_{33}}} \times \left[d + h_u \left(\frac{\varepsilon_{||}}{\varepsilon_g} - 1 \right) + h_g \left(\frac{(\varepsilon_{||} - \varepsilon_g)X}{\varepsilon_g X + \varepsilon_{||} Y} \right) \right] \quad (1)$$

That is, voltage required to latch from C to D states V_{CD} is related to the pulse duration τ, cell gap d, flexoelectric coefficients e_{11} and e_{33}, twist viscosity γ_1, surface viscosity l, surface zenithal anchoring energy W_θ, dielectric anisotropy $\Delta\varepsilon$ and bend elastic constant K_{33}. The expression also includes terms for the dielectric effect of the grating approximated to a shape of amplitude h_g, offset h_u, dielectric constant ε_g, full-width half maximum X, and pitch X + Y, as shown in Figure 3.

Figure 4 compares the results for the latching voltage dependence on cell gap and grating zenithal anchoring energy calculated from full numerical modelling with those found using Eq. (1), indicating how well the simple expression works in practice [4]. However, the grating terms in this expression relate to the dielectric effect of the grating only, and do not express the effect of shape differences on the defect dynamics. Hence, either numerical or experimental approaches are required to understand the effect of grating shape, and it is the latter approach that is taken here.

3. Experimental Details

Liquid crystals cells of the present study were fabricated using the same procedure as that used for commercial devices. Low cost fabrication of the grating on the LCD

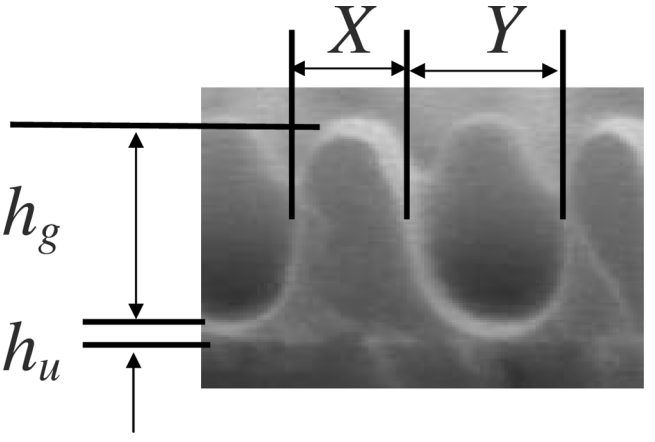

Figure 3. Parameters used to define a simplified grating shape.

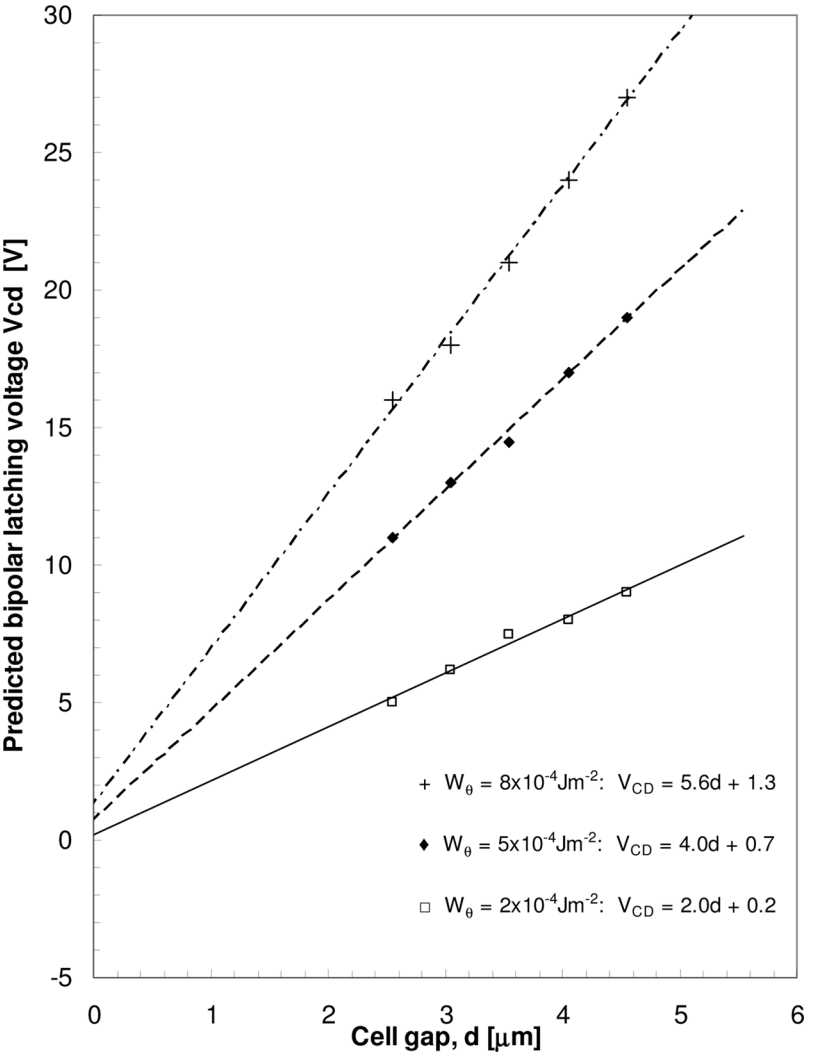

Figure 4. Latching voltage dependence on cell gap and anchoring energy predicted from the full numerical model and Eq. (1).

mother glass uses simple embossing, in which a photo-lithographically defined master structure is copied, first into Nickel shims, and then onto a roll of film supplied to the LCD manufacturer. The grating is then replicated in the LCD factory into a suitable photo-polymer on the internal surface of the display by simple UV embossing [2] combined with a self-patterning method based on selective adhesion [6]. Firstly, the LCD mother glass is printed with a UV curable adhesion promoter to define the areas to be patterned with the grating (the display viewing areas) and ensure that the areas of the plate that form the glue seal and bonding ledges are devoid of the grating. A homeotropic photopolymer with the required zenithal anchoring energy is then deposited onto the edge of the LCD mother glass and the grating film then placed on top. The plate-photopolymer-film sandwich is then embossed

between rubber rollers at a speed sufficiently slow and pressure sufficiently high to ensure that the offset h_u (and hence unnecessary voltage drop) is kept to a minimum without damaging the grating structure. The photopolymer is cured by exposure to UV from a simple uncollimated source. This polymerises the grating material, but also bonds the underside of the grating to the adhesion promoter. The film surface is arranged to give stronger adhesion to the surface of the photopolymer than between the photopolymer and glass, but far lower than the adhesive force of the adhesion promoter to the glass. With this arrangement, peeling of the film from the cured motherglass automatically patterns the plate, so that unwanted areas of photopolymer are stripped away with the film. The grating mother glass is then combined with a standard patterned rubbed polymer plate, spaced using appropriate glass bead spacers and glue seal to form a glass laminate in the conventional fashion. The cells are then completed by scribing and vacuum filling with liquid crystal.

The tooling chain of nickel and film faithfully replicates the original master. The master gratings used in the current work were produced using hard-contact photolithography, using a chrome on quartz mask. Grating shape was varied both by altering the mark to space ratio of the mask, and by varying master processing conditions such as resist material, thermal processes and UV exposures.

4. Results

A typical ZBD has a pitch and grating depth of around 1 micron. However, bistability exists for a broad range of different grating shapes which can be realised by careful design of the photo-mask and photolithographic process conditions used to make the master structure. Shapes containing either single convex and concave surface features (such as sinusoidal or triangular shapes) or multiple convex and concave surface features (such as trapezoidal or more complex shapes) are possible. Furthermore, the sidewall angles and asymmetry can also be controlled through careful choice of exposure conditions and thermal processing. Grating pitch and duty cycle can be independently varied through mask design and process conditions. Variation in the structure along the groove direction are also possible through mask design which can provide benefits to the operating temperature range. Variations to the grating shape within each pixel can be used to create greyscale [7].

4.1. *Pre-Tilt*

The elastic distortion of the director field around the grating in the continuous C state decays into the bulk, resulting in vertical alignment for a symmetric grating, and near vertical alignment for a blazed grating. Modelling shows that the deviation from vertical is minute even when the degree of blaze is considerable [1]. Conversely, the pre-tilt of the D state is sensitive to grating shape being dictated by the relative separation of the +/− ½ defects [2]. A periodic grating is preferred, since this leads to a uniform pre-tilt and optical appearance. The pre-tilt is then:

$$\theta_{\mathrm{D}} = \pi/2 - \mathrm{a/L} \tag{2}$$

where a is the distance between $+1/2$ and $-1/2$ disclinations and L is the grating pitch, as shown in Figure 5. For the simple blazed sinusoidal gratings the D state

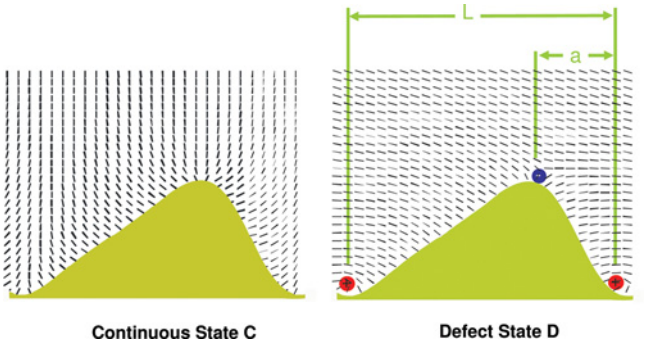

Figure 5. Pre-tilt in the C and D states and the relationship to blaze. (Figure appears in color online.)

pre-tilt is related to the degree of blaze. Figure 6 shows the excellent agreement between experimental pre-tilts measured using crystal rotation for a series of different grating shapes with the values predicted from Eq. (2), wherein the shape factors a and L were determined using SEM measurements from the grating.

Trapezoid grating shapes give multiple defect positions, thereby allowing multi-stable pre-tilts to be defined. Gratings with D state pre-tilts ranging from 0°to 55° have been produced in practice. For the ZBD devices operating in the TN mode, a pre-tilt of about 5 to 10° is ideal to give no reverse TN tilt/twist domains whilst ensuring an excellent viewing angle. This is achieved using grating shapes that are near sinusoids, and such shapes are used throughout the rest of this work.

Pre-tilt variation across the grating area may become manifest as a change in appearance (for example, changing brightness and/or viewing angle for a device with a Normally White TN for the D state). Variations in grating peak width generally follow the variation in chrome width on the photo-mask, the UV light intensity

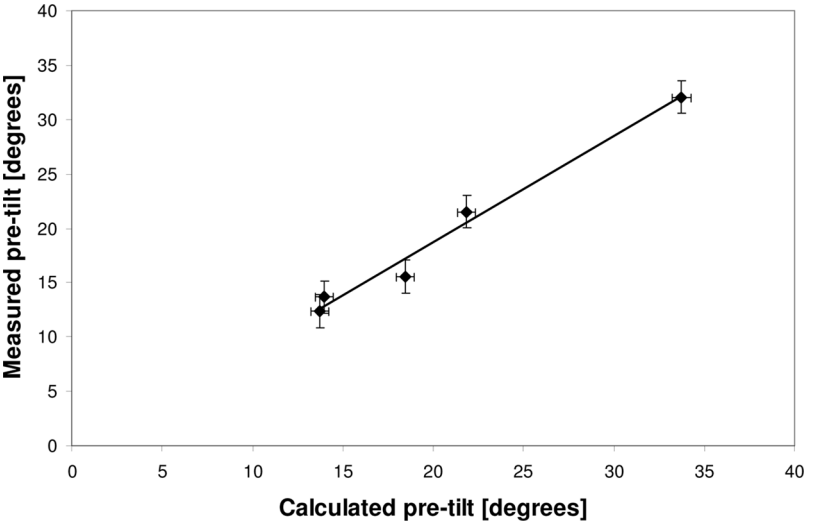

Figure 6. Measured pre-tilt and calculated pre-tilt using Eq. (2).

uniformity and temperature uniformity. Typical chrome range for a ZBD production mask is 20 nm. The ZBD mastering process uses a UV light source with <2% variation and the thermal processing is performed with <1% variation. The combination of these three factors lead to a variation in pre-tilt of only +/− 1.5 degrees for a typical grating with a pre-tilt average of about 6 degrees: this variation is far too small to cause any observable difference in the optical properties of the D state.

4.2. *Temperature Range*

The operating temperature range of the ZBD device is a complicated issue, relating to the liquid crystal properties, the addressing waveforms and the grating shape and material. However, the basic range over which bistability is maintained is dictated to a large extent by grating shape. Bistability occurs not just where the elastic deformation energies of the C and D states are equivalent, but for a range of temperatures over which the energy barrier between the states is greater than thermal, mechanical and electrical fluctuations that the device may be subjected to. In practice, the bistable temperature range may be as low as 20°C, for a simple mono-grating structure, outside of which one of the states will tend to spread into areas previously latched into the opposite state. Consider the boundary between areas of C and D states. The disclination pair of the D state forms a loop, and at the boundary the $+1/2$ defect moves away from the grating trough and the $-1/2$ defect moves away from the grating ridge to meet at some intermediate point on the surface. Any disturbance to that defect loop can readily cause the point of annihilation to move, causing one state to spread into the other undesirably.

The solution to this is to create breaks along the length of the grating every few microns or so. An effective break is a 180° phase shift, or slip, as shown in Figure 7. The slip provides vertical concave and convex edges to the defect loops, providing a defined point at which the boundary between states can occur. Providing slips periodically every few microns along the length of the grating ensures that the two

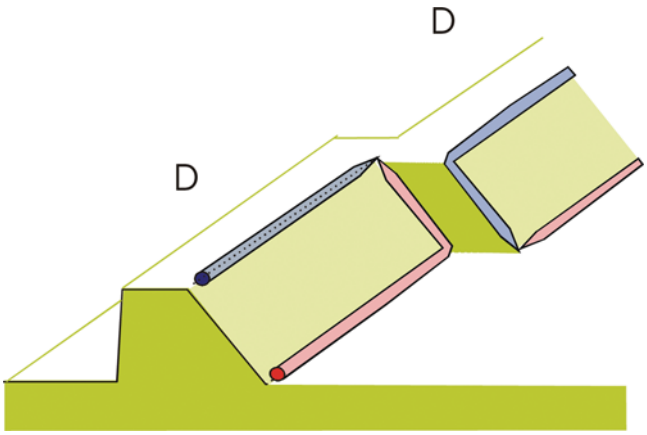

Figure 7. Schematic representation of a grating slip, used to stabilise the C and D states across a wide temperature range. (Figure appears in color online.)

states can be maintained to within a few degrees Celsius of the clearing temperature, and bistable ranges from −30°C to +80°C have been realised in practice.

4.3. *Latching Voltages*

Figure 8 shows the experimentally obtained latching voltages for the liquid crystal material B from reference [8] operating in a 5 μm cell gap for different grating shapes (a range of grating amplitudes $0.8 < A < 1.2$ μm; grating duty cycles $0.34 < FWHM/P < 0.46$ and grating pitches $0.6 < P < 1.4$ μm). The results suggest that lower voltage

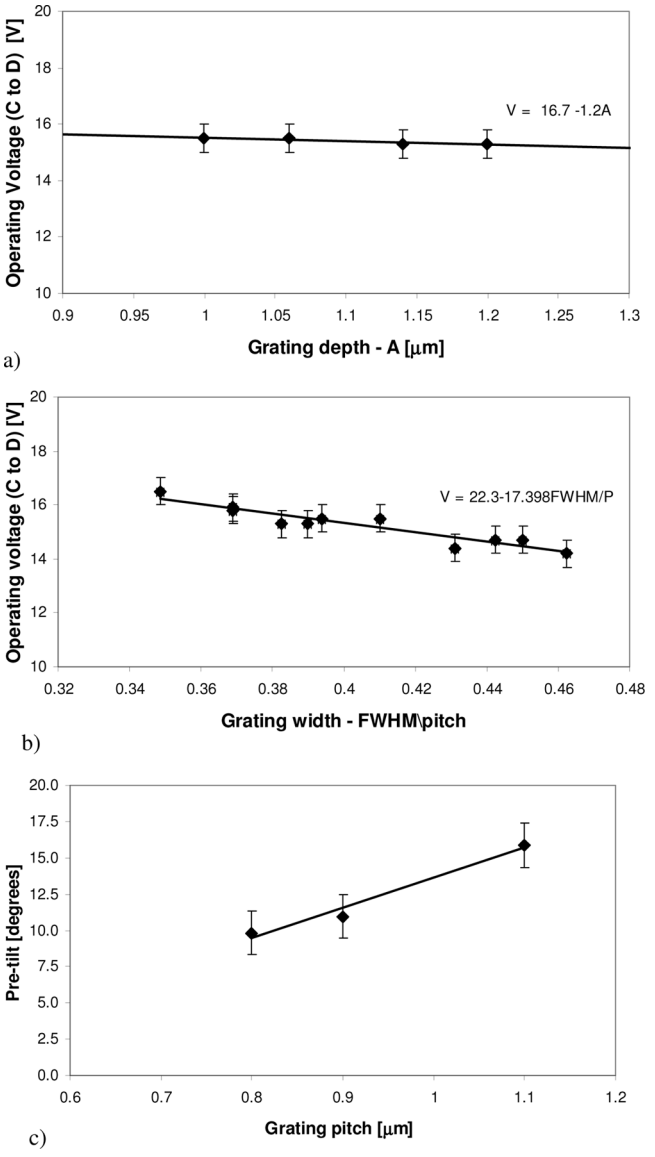

Figure 8. Experimental latching voltages V_{CD} for (a) varying grating amplitude h_g; (b) varying grating width $FWHM/P = X/X + Y$; and (c) varying pitch $P = X + Y$.

operation can be achieved by using shorter pitch gratings with a narrower groove. In practice, the choice of grating shapes are limited by the critical dimension tolerances of the photo-mask used to produce the master, and the mechanical properties of the nickel and film used to tool the grating. A pitch of 0.8 μm, formed from a 360 nm ridge and 440 nm groove gives satisfactory compromise between manufacturability and performance. Figure 9 shows the excellent fit between the numerical theory and the experimental τV latching response for cells constructed with two different FWHM values.

A strong factor influencing the operating voltage is the anchoring energy of the photo-polymer used to form the grating. Figure 10 shows the direct relationship between latching voltages and anchoring energy, which was determined by comparing the cell gap dependences with the numerical results [4]. Homeotropic anchoring

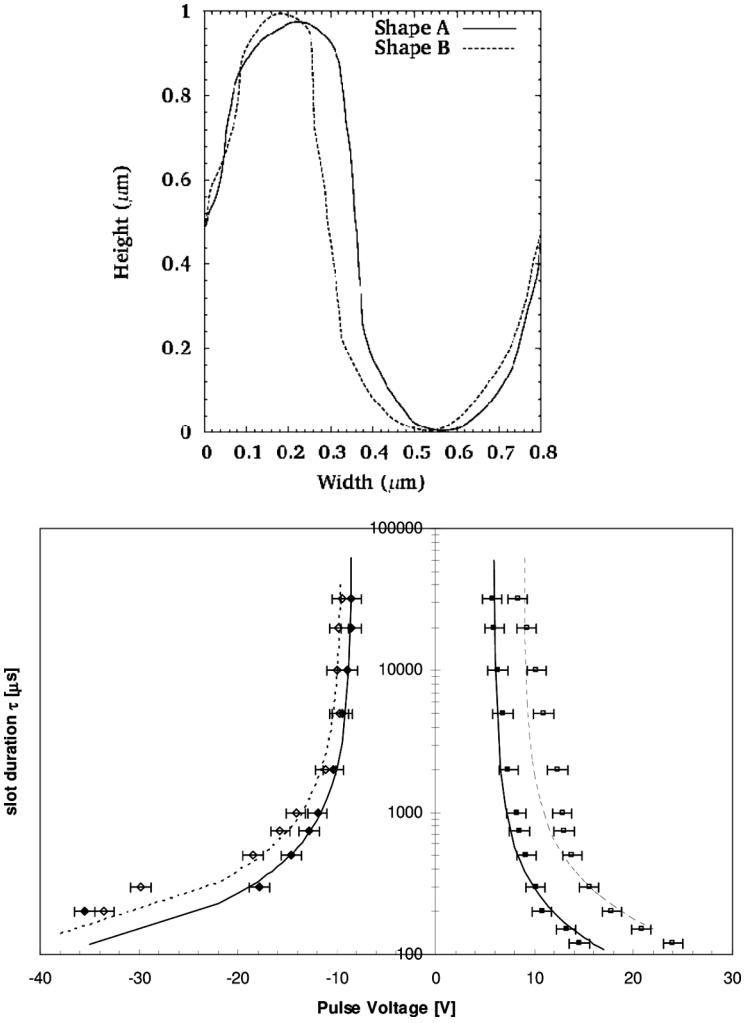

Figure 9. Cubic spline of two experimental grating shapes, and the comparison of theoretical and experimental τV resulting from those shapes.

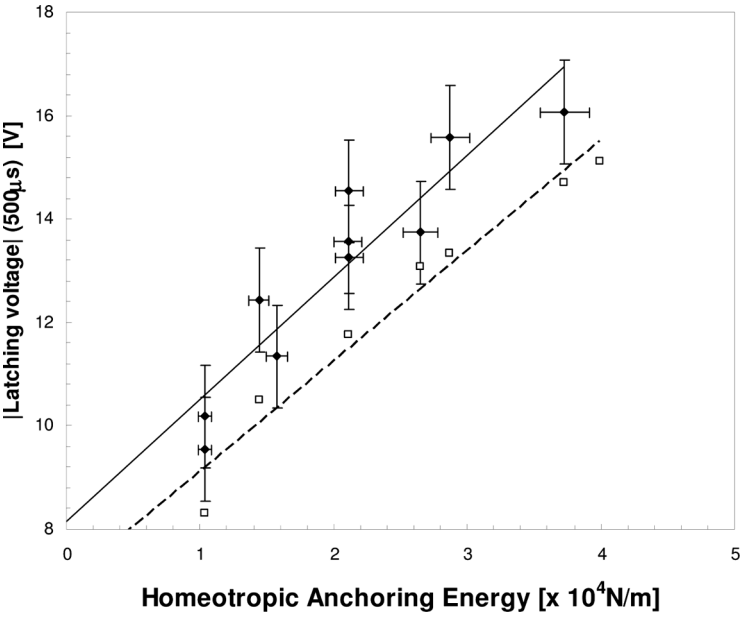

Figure 10. Experimental relationship between latching voltages and grating zenithal anchoring energy.

energies W_θ below 1×10^{-4} N/m were found both experimentally and in the model, to not sustain zenithal bistability. Higher anchoring energies lead to high operating voltages, and so in practice, choosing a material with $W_\theta \approx 2 \times 10^{-4}$ N/m gave good device performance.

Understanding how device performance depends on both shape and surface anchoring energy is vital to enable high yield manufacture. Small changes in grating shape can arise when using different photo masks or masters, nickel tooling or different manufacturing process parameters (such and temperature or UV light intensity for example). These unavoidable variations in shape and process conditions can be precisely compensated for by appropriate choice of surface anchoring energy.

5. Conclusions

Both empirical and theoretical methods have been employed to optimise the grating shape and anchoring energy for application in actual devices. Both shape and uniformity optimisation throughout each fabrication step has resulted in a low-cost high-yielding volume manufacturing process. The results from this study have already been used to provide the excellent performance and uniformity of the ZBD devices being used in retail applications.

References

[1] Bryan-Brown, G. P., Brown, C. V., & Jones, J. C. (1995). US Patent 06249332.
[2] Jones, J. C. (2008). *Journal of the SID*, *16*, 143–154.
[3] Spencer, T. J., & Care, C. M. (2006). *Phys. Rev. E*, *74*, 061708.

[4] Spencer, T. J., Care, C. M., Amos, R. M., & Jones, J. C. (2010). *Phys. Rev. E*, *82*, 021702, 1–13.
[5] Davidson, A. J., & Mottram, N. J. (2002). *Phys. Rev. E*, *65*, 051710.
[6] Bryan-Brown, G. P., Walker, D. R. E., & Jones, J. C. (2009). *SID Symposium Digest*, *40*(3), P65, 1334–1337.
[7] Jones, J. C., Beldon, S. M., & Wood, E. L. (2003). *J. Soc. Inf. Disp.*, *11*, 269.
[8] Jones, J. C., Beldon, S. M., Francis, M., & Goulding, M. (2003). *SID Symposium Digest*, *34*(2), 26.2, 954–957.